Available online at www.sciencedirect.com
ScienceDirect
Journal of Luminescence 121 (2006) 249–255
JOURNAL OF LUMINESCENCE
www.elsevier.com/locate/jlumin

Optical losses and gain in silicon-rich silica waveguides containing Er ions

D. Navarro-Urrios[a], M. Melchiorri[a], N. Daldosso[a,*], L. Pavesi[a], C. García[b], P. Pellegrino[b], B. Garrido[b], G. Pucker[c], F. Gourbilleau[d], R. Rizk[d]

[a]*Laboratorio Nanoscienze, Departimento di Fisica, Università di Trento, Via Sommarive 14, I-38050 Povo (Trento), Italy*
[b]*EME, Departament d'Electrònica, Universitat de Barcelona, Martí i franquès, 1, 08028 Barcelona, Spain*
[c]*ITC-irst, MT Lab, Via Sommarive 18, I-38050 Povo (Trento), Italy*
[d]*SIFCOM, UMR CNRS 6176, ENSICAEN, 6 Boulevard Maréchal Juin, 14050 CAEN, France*

Available online 18 September 2006

Abstract

Rib-loaded waveguides containing Er^{3+} coupled to Si-nc have been produced by magnetron sputtering and successive thermal annealing to investigate optical gain at 1535 nm. It has been shown that all Er ions are optically active, whereas the fraction that can be excited at high pump rates under non-resonant excitation is strongly limited by confined carrier absorption (CA), up-conversion processes, and mainly by the lack of coupling to the Si-nc. Er^{3+} absorption cross-section is found comparable to that of Er^{3+} in SiO_2, but a dependence with the effective refractive index has been found. Although the presence of Si-nc strongly improves the efficiency of Er^{3+} excitation, it introduces additional optical loss mechanisms, such as CA. These Si-nc losses affect the possibility of obtaining net optical gain. In the present study, they have been minimized by lowering the annealing time of the Er-doped Si-rich oxide. In pump–probe measurements it is shown that signal enhancement of the transmitted signal can be achieved at low pumping rate when the detrimental role of confined CA is attenuated by reducing the annealing time. A maximum signal enhancement of about 1.30 at 1535 nm was observed.

Keywords: Er amplifier; Si photonics; Waveguides; Gain; Absorption cross-section

1. Introduction

The interest on erbium-doped waveguide amplifiers (EDWAs) comes from the deployment of local-area optical links where planar photonic integrated circuits are used. In EDWA, Er^{3+} is inserted in a silica matrix and amplification occurs in the technologically relevant 1.55 μm wavelength region. But in order to invert the erbium population one has to use powerful lasers finely tuned within an erbium transition, whose absorption cross-sections are quite low, and no electrical pumping is possible [1]. The use of erbium sensitizers can relax these stringent and unfavorable pumping conditions. Silicon nanoclusters (Si-nc) coupled to Er ions is one of the more interesting Er sensitizers.

In fact, a heterogeneous material in which Si-nc embedded in a silica matrix doped with Er has shown a combination of the good properties of the dielectric-doped [2] and semiconductor-doped mediums [3–9]. In particular, Er-doped bulk Si shows an efficient transferring of the excitation from electron–hole pairs excited in silicon, which can be performed either by optical pumping or by electrical injection. Er in bulk Si have strong non-radiative recombination paths that compete with the radiative ones, quenching the Er emission at room temperature [3].

These limitations are not present when Er is coupled to Si-nc formed in silica. Si-nc strongly absorb light in the visible range ($\sigma = 10^{-16}\,cm^{-2}$ in the visible range) [3–9] by formation of excitons, whose energy is rapidly ($<1\,\mu s$) and efficiently ($>60\%$) transferred to the Er ions via an Auger mechanism [10,11]. Another important role of the Si-nc is to allow easy fabrication of waveguides where the average refractive index of the core is determined by the size and

*Corresponding author. Tel.: +39 0461882030; fax: +39 0461881696.
E-mail address: daldosso@science.unitn.it (N. Daldosso).

0022-2313/$ - see front matter © 2006 Elsevier B.V. All rights reserved.
doi:10.1016/j.jlumin.2006.08.002

density of Si-nc, thus allowing a good light confinement. Finally, electroluminescence has been repeatedly reported in the Er coupled to Si-nc in silica material system, which opens the route towards an electrically pumped optical amplifier [12].

In this work we address some of the problems encountered when trying to achieve good amplification performances: up-conversion, confined carrier absorption (CA) and effective density of Er ions coupled to the Si-nc.

2. Waveguide fabrication and experimental details

Er^{3+}-doped Si-nc silica waveguides have been prepared by a multi-wafers reactive magnetron co-sputtering of a pure silica target topped with Er_2O_3 pellets. The incorporation of Si excess in the film was obtained by mixing the plasma with hydrogen, owing to its ability to reduce the oxygen provided by the silica target. The hydrogen rate (mixed to argon) was kept to 60% while the Si substrates, on which a 15 μm thermal SiO_2 layer was previously grown, were not intentionally heated. More details on the process can be found elsewhere [13]. After the deposition of 1 μm-thick Er/silicon-rich oxide (SRO) layer, a 1 μm-thick SiO_2 cladding layer has been deposited by sputtering a SiO_2 target in pure argon plasma. Then the wafers have been annealed for different times at 900 °C under pure N_2 flux to activate Er^{3+} ions, to induce the precipitation of the Si excess into nanoclusters and to improve the energy transfer between the Si-nc and the Er^{3+} ions. The annealing temperature was chosen on the basis of previous optimization studies [13,14]. The annealing duration has been varied between 1 and 240 min: annealing times longer than 60 min have shown no improvement in the optical properties of Er-doped Si-nc systems. This annealing time variation aimed at reducing the Si-nc size thus reducing the CA within the Si-nc. Secondary ion mass spectroscopy (SIMS) and Rutherford backscattering spectroscopy (RBS) have been performed to determine Si and Er content (see Table 1).

Optical lithography and reactive ion etching have been used to define 2–3 cm long rib-loaded waveguides with rib widths ranging between 3.5 to 12 μm. It is worth noting here that the very low refractive index of the 5 and 1 min annealed films results in no light confinement in the 1500–1600 nm range. On the contrary, waveguides annealed at 60 (from now sample B), 30 (sample C) and 10 min (sample D) have calculated optical confinement factors Γ of the fundamental mode at 1535 nm of 0.51, 0.48 and 0.28, respectively, for a rib width of 12 μm.

Photoluminescence (PL) measurements have been performed by pumping with the 476 nm (out of Er resonance pumping conditions) and 488 nm (resonance pumping conditions) lines of an argon laser and detecting light with a monochromator coupled to an InGaAs photomultiplier. Total lifetime measurements were done by chopping the pump and connecting the output of the photomultiplier to a digital oscilloscope.

Internal gain measurements of the rib-loaded waveguides have been performed by butt-coupling signal light through a single-mode polarization-preserving tapered fiber moved by a piezo-electric stage. The light exiting the end facet of the waveguide was observed with a microscope objective matched, through a prism beam splitter, both to a zoom mounted on an InGaAs camera and to a Ge detector. We have used two different signal light sources: a tunable laser (1.5–1.6 μm) that cover the $^4I_{13/2} \rightarrow {}^4I_{15/2}$ internal Er^{3+} transition (peaked at 1535 nm) and a diode laser operating at 1310 nm, well away from transitions related to Er^{3+} ions. The pump source was a Millenia laser (532 nm, up to 10 W) focused on the waveguide surface into a stripe 100 μm wide and 1 cm long by means of a cylindrical lens. The alignment of the pump beam stripe and the rib-loaded waveguide was checked by two cameras which allow observing both the waveguide surface and exiting facet. It has to be considered that the pumping wavelength is not strongly resonant with any Er^{3+} absorption transitions. Some measurements were done by using the 488 nm line of an argon laser, resonant with an Er^{3+} absorption peak [$^4I_{15/2} \rightarrow {}^4F_{7/2}$], for comparison. In order to eliminate the diffused light and the amplified spontaneous emission (ASE) parasitic signal, the weak probe signal was chopped (10 kHz) and measured through a lock-in system.

3. Refractive index dependence on the annealing time

We characterized the waveguide parameters of each sample with the m-line prism coupling technique. The coupling region between the sample and prism was illuminated with the 633 nm line of a He–Ne laser at variable angle. The angular dependence of the reflectance of the beam is measured, and each time the light couples with a guided mode in the waveguide it observed a sharp dark peak, thus the effective index of each mode is calculated as a function of the incident angle. With this method it is possible to assess independently the core layer

Table 1
Sample parameters: annealing time, Si excess, Er content, up-conversion coefficient, refractive index n at 632.8 nm, fundamental mode optical confinement factor Γ

Waveguide sample	Annealing time (min)	Si excess (at%)	Er content ($\times 10^{20}\,cm^{-3}$)	C_{up} ($\times 10^{-17}\,cm^3\,s^{-1}$)	n	Γ
B	60	7	4 ± 0.1	2.0	1.545	0.51 ± 0.02
C	30	6–7	5.4 ± 0.2	5.5	1.516	0.48 ± 0.02
D	10	6–7	5.4 ± 0.2	8.0	1.48 ± 0.01	0.28 ± 0.03

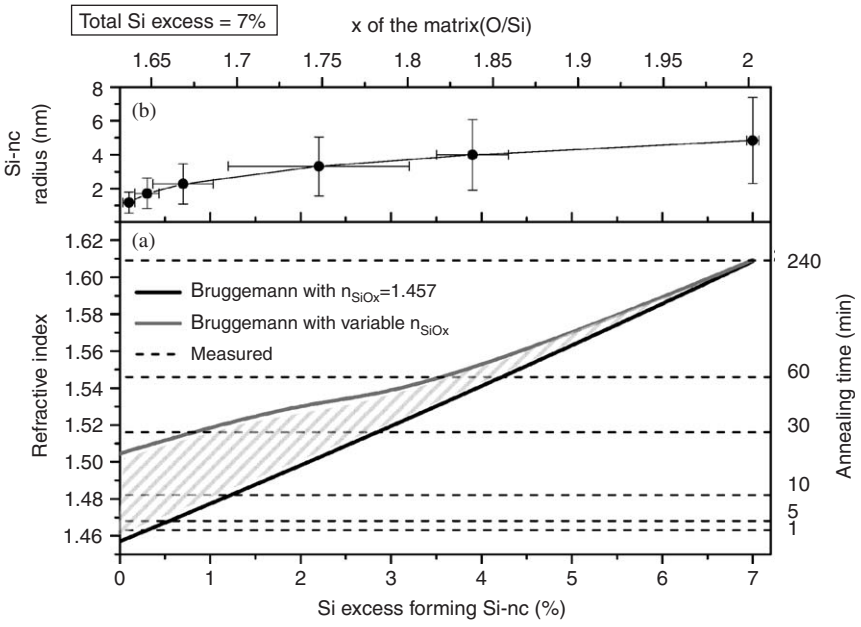

Fig. 1. Panel (a): two-component Bruggemann calculation using SiO_2 refractive index of 1.457 (black line) and using the refractive indices of SiO_x found in literature as a function of x (gray line). Dashed lines correspond to the measured refractive indices of the different samples. Panel (b) plots the dependence between the radius of Si-nc and the silicon excess forming part of Si-nc for a Si-nc density of $1–5 \times 10^{17}\,cm^{-3}$.

thickness d and the refractive index n [15]. A decrease of n while reducing the annealing time was observed (dashed lines in Fig. 1). d was different from sample to sample: 880, 890, 840, 840, 750 and 750 nm for wafers annealed at 1, 5, 10, 30, 60 and 240 min, respectively. The decrease of the core layer thickness is related to the well-known phenomena of film densification.

The Si content of the film (7% Si excess in all the samples) measured by RBS and SIMS does not change as a function of the annealing time. In order to know how it is incorporated to form Si-nc as a function of the annealing time we consider that a fraction of all the Si excess is clustering into Si-nc and another fraction is still incorporated into the dielectrics surrounding the Si-nc (matrix); this in turn means that the matrix is not stoichiometric SiO_2 but sub-stoichiometric SiO_x, where the actual value of x ($1.63 \leqslant x \leqslant 2$) depends on how much Si has been clusterized. By changing the annealing time, Si-nc grows and the fraction of Si incorporated into them increases.

Therefore, we consider that the core layer is composed by Si-nc (dielectric permittivity ε_1) embedded into a matrix of sub-stoichiometric defected silica phase SiO_x ($\varepsilon_2(x)$). In order to have the refractive index of SiO_x as a function of x, we have taken several values from the literature [16] and performed an interpolation by using a polynomial fit. Then, we have applied the two-component Bruggemann formula which gives the effective dielectric constant of the core layer ε_{eff} by solving the implicit equation [17]:

$$f\frac{\varepsilon_1-\varepsilon_{eff}}{\varepsilon_1+2\varepsilon_{eff}}+(1-f)\frac{\varepsilon_2-\varepsilon_{eff}}{\varepsilon_2+2\varepsilon_{eff}}=0, \quad (1)$$

f being the volumetric fraction of Si within the Si-nc. A simplifying assumption has been used that the two phases have the same mass density ($\sim 2.3 \times 10^6\,g/m^3$). From $\varepsilon_{eff} = n^2$, we infer the refractive index of the core layer.

The results of our modeling are reported in Fig. 1 as a function of the percentage of excess Si precipitated into the Si-nc. The gray curve is an upper limit of the real situation where it is assumed that the Si-nc are embedded in a sub-stoichiometric silica (n variable) in which the total Si excess of the sample is constant as we have explained before. The bottom panel of Fig. 1 can be read as follows: 0% means that no Si is incorporated into Si-nc, i.e. no Si-nc were formed, and thus the matrix has a composition of $x = 1.63$. This case describes the as-deposited film. Then by annealing, the Si-nc grows and thus x increases due to the incorporation of Si into Si-nc. The limit is when all the excess Si is incorporated into the Si-nc and this occurs when the matrix becomes pure stoichiometric silica with $x = 2$.

A lower limit for the real situation is represented by the black line, which refers to a situation where the refractive index of the matrix is considered constant and equal to that of silica ($n = 1.457$) and all the Si excess is a variable incorporated to the Si-nc (the total Si excess in this curve is not constant).

By using this model and looking at the crossing value between the measured refractive index (dashed lines) and the calculated refractive index (lines) it is possible to deduce the fraction of Si which is incorporated into the Si-nc for the various annealing times we used. The accuracy of our estimate is given by the interval comprised between the

gray and the black lines. For short annealing time, we found that the gray line is systematically larger than the measured refractive indices. This is due to the presence of voids in the core layer. We have calculated, by using a three-component Bruggemann relation [18], that with a voids density of 6% in volume in the samples, the refractive index of the gray line is reduced to 1.46 in the as-deposited sample. These voids are eliminated by increasing the annealing time due to the densification of the layer.

On the contrary, for the longest annealing time, the SiO_x phase is practically stoichiometric and n is modeled accurately by assuming that all the Si excess has been consumed by the Si-nc formation and the embedding matrix is formed by pure and defect-free SiO_2. This is manifested by the fact that the gray and black lines meet together and with the experimental point.

The modeling shown in the bottom panel of Fig. 1 indicates that the increase of n with annealing time is due to the increased phase separation between Si and SiO_x and to the growth of the Si-nc sizes. If we assume that the Si-nc growth occurs at nucleation seeds whose density depend mainly on the annealing temperature (fixed at 900 °C), the Si-nc density (N_{nc}) is independent on the annealing time once nucleation is settled in and the increase of n can be mainly explained by an increase of the Si-nc volume (V_{nc}) or the Si-nc size. An estimate of the Si-nc size can be done if we assume a constant density of Si-nc ($1–5 \times 10^{17}\,cm^{-3}$). The results are shown in the top panel of Fig. 1.

4. Losses measurements and emission cross-sections

In the past some controversial assessments of the emission (σ_{em}) and absorption (σ_{abs}) cross-sections of Er coupled to Si-nc have been reported. Here we show that the emission cross-section of the $^4I_{13/2} \rightarrow {}^4I_{15/2}$ transition of the Er^{3+} ions is not significantly enhanced by the presence of the Si-nc and that only weak differences due to the

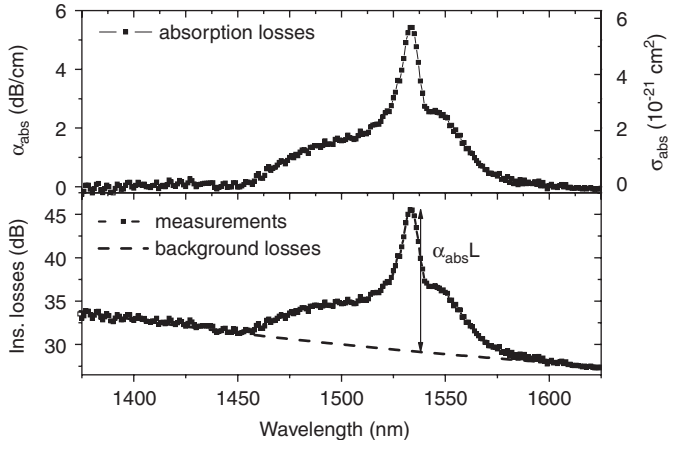

Fig. 2. (Bottom panel) Insertion losses (squares) and background losses (dashed line) for sample B. (Top panel) Absorption losses (left) and absorption cross-section (right) obtained following the explained procedure.

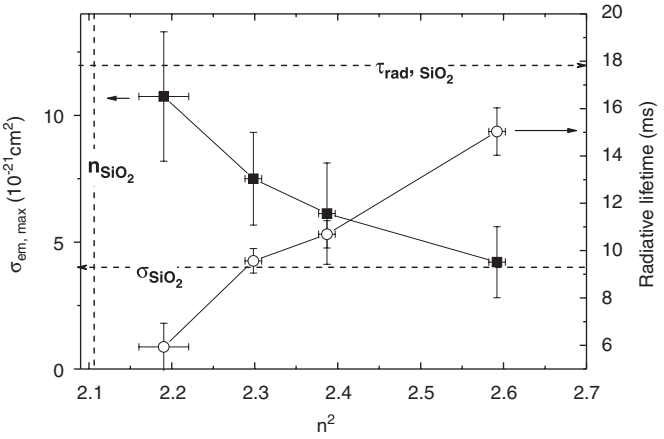

Fig. 3. Cross-section peak (left) and radiative lifetimes (right) as a function of the square of the refractive index n. Data for Er^{3+} in SiO_2 taken from the literature are also plotted as straight lines.

variation of the effective refractive index are observed. With the aim of extracting the absorption cross-section, the losses of sample have been measured by the insertion loss technique [19]. Far from the Er^{3+} absorption, the losses are only due to the scattering which can be described by the Rayleigh scattering law. In Fig. 2 we show the insertion losses results for sample B. At 1535 nm we obtain absorption losses (α_{abs}) of 5.4, 8.5 and 7.5 dB/cm for samples B, C and D, respectively [20]. By using the optical confinement factor and considering that all the erbium ions are optically active [21], it is possible to extract σ_{abs}. The emission cross-section spectral dependence can be obtained in a quantitative manner by the low pumping rate luminescence spectra by using [22].

$$\sigma_{em}(\upsilon) = \sigma_{abs}(\upsilon) e^{\varepsilon - h\upsilon/kT}, \tag{2}$$

where ε is the transition energy between the lowest levels of the two manifolds involved and T the sample temperature. In order to obtain σ_{em} we have normalized the luminescence spectra at low pump power to the maximum value of σ_{abs} for each waveguide. We have found that the spectral σ_{em} lineshapes change and the σ_{em} strength slightly decreases by increasing the annealing time. This has been interpreted as a change in the interaction of Er^{3+} with the field of the embedding medium (local field effects). In Fig. 3 (left-axis) we show that, since Er^{3+} is in the oxide, as the phase separation progresses Er^{3+} is surrounded more and more by a pure SiO_2 environment. Consequently, σ_{em} tends to the value for Er^{3+} in pure silica.

In Fig. 3 (right-axis) we evidence the relevance of local field effects since the radiative Er^{3+} lifetime is increasing as a function of n^2. It is interesting that on waveguide sample annealed for 240 min, which is completely phase separated (thus giving the higher refractive index) and where the dielectric has a high quality, we have obtained a radiative lifetime which is smaller than the literature value for Er in pure silica. This can be explained in terms of mean field variations, which means a larger n.

5. Lifetime measurements

Luminescence decay measurements at 1535 nm for samples B, C and D have been performed as a function of the photon flux. The Er^{3+} lifetime at low photon flux increases significantly with annealing time while σ_{em} decreases. The increase of the radiative lifetime reported in Fig. 3 is not enough to explain this. Other non-radiative recombination paths such as defects in the matrix or up-conversion recombinations between close Er^{3+} ion pairs play an important role.

In order to clarify the effects of up-conversion, we have fit the experimental PL decay by solving the differential equation that rules the decay rate of the Er^{3+} excited level population N_2 taking into account the cooperative up-conversion:

$$\frac{dN_2(t)}{dt} = \frac{N_2(t)}{\tau_d} - C_{up}N_2(t)^2, \tag{3}$$

where τ_d is the Er^{3+} lifetime, which counts for the radiative and the N_2 independent non-radiative recombination paths. C_{up} is the up-conversion coefficient between pairs of excited ions.

In Fig. 4, the experimental measured temporal dependence of N_2, deduced from the PL decay, for sample B is reported. N_2 was normalized to the steady state population generated at different fluxes. At low excited erbium concentration (low pumping fluxes) the decays are single exponentials while increasing the pumping flux the decays seem to become faster in the first few ms. By using τ_d and C_{up} as parameters, we fitted the N_2 decays for each sample. The results, reported in Table 1, are that up-conversion becomes more important as the annealing time reduces.

From the found up-conversion coefficients we can estimate the effects that up-conversion has on the population inversion. For example in sample B, the presence of up-conversion increases the photon flux needed to reach population inversion (threshold flux) by one order of magnitude. If we assume that the effective excitation cross-section of Er is of the order of $1 \times 10^{-16}\,cm^2$, a threshold flux of 2×10^{18} (ph/cm^2 s) would be needed in absence of up-conversion. This shows that in presence of up-conversion, the Si-nc are still effective and makes the threshold flux much lower than that needed in a directly pumped erbium system [2].

6. Signal enhancement

We report here amplification studies by using the signal enhancement factor SE, which is equal to the ratio of the transmitted intensity under pumping conditions (I_{PP}) to the transmitted intensity without pump (I_P). To model $SE = I_{PP}/I_P$, we approximate the physical system as a two level system and we work in the regime of weak probes [23], then

$$SE = \exp(2\sigma_{em}N_2\Gamma L) \approx \exp\left[\left(\frac{2\Phi\sigma_{exc}}{1/\tau_d(\Phi) + \Phi\sigma_{exc}}\right)\sigma_{em}NL\Gamma\right], \tag{4}$$

where τ_d is the lifetime of the excited level, L the pumped length and N and N_2 the total and first excited state ion concentration, respectively. Note that we have explicated the Φ dependence of τ_d because of possible non-radiative effects, such as up-conversion or excited state absorption, which are photon flux density dependent. It is worth noting also that we have made the approximation of taking $1/\tau_d = 1/\tau_d(\Phi\downarrow) + C_{up}N_2(t=0)$. The internal gain coefficient in cm^{-1} will be defined as $g = \sigma_{em}N_2\Gamma$.

Fig. 5 reports the signal enhancement at a wavelength of 1310 nm as a function of Φ. Er^{3+} does not have any absorption resonance at this wavelength. Thus the decreasing

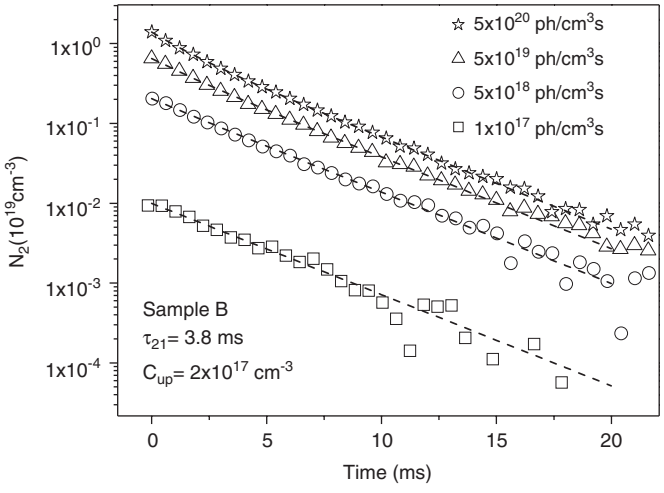

Fig. 4. Measured (symbols) and simulated (dashed lines) temporal decays of the number of excited Er for sample B. Different starting pumping fluxes have been used.

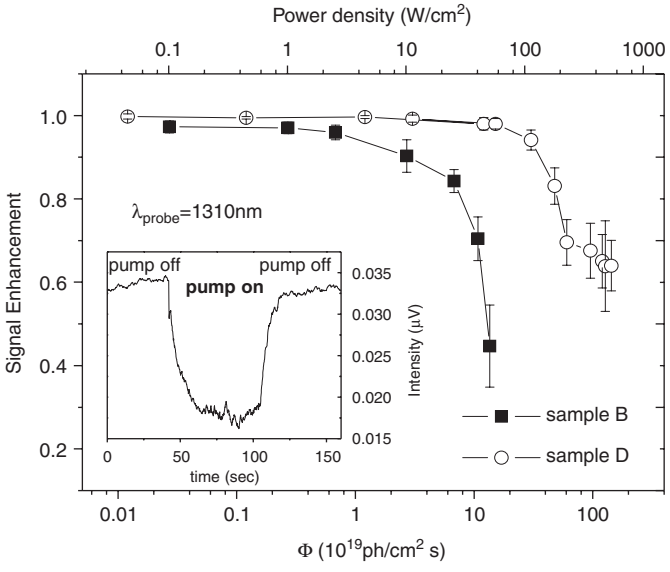

Fig. 5. Measured signal enhancement using a 1310 nm probe for sample B (black squares) and sample D (empty circles). Inset: the time dependence of the SE. The pump wavelength was 532 nm.

SE can be explained by confined CA in the Si-nc. Confined CA is a mechanism which depletes the Si-nc and, as a consequence, introduces a new loss mechanism and probably also quenches the excitation of Er^{3+} via Si-nc [19]. When decreasing the annealing time from 60 to 10 min, we have significantly decreased this detrimental CA process. In fact, SE = 0.7 at a $\Phi = 1 \times 10^{20}$ ph/cm^{2}s for sample B while we obtain the same attenuation for $\Phi = 6 \times 10^{20}$ ph/cm^{2}s for sample D. The inset of Fig. 5 shows the time dependence of SE: it has long turn-on and turn-off times. These long times cannot be explained by the lifetime of excitons in Si-nc, which is of the order of tens of microseconds. As suggested in Ref. [24], these long lifetimes can be explained by excitons which are formed by electrons and holes separated by a large distance. There are two possibilities: the carriers are localized (1) within the same Si nanocluster or (2) in nearby ones. The first mechanism is related to the size of the Si-nc whereas the second with the distance between the Si-nc.

When using a signal at 1535 nm, we are probing the Er^{3+} absorption band. Fig. 6 reports the measured SE as a function of Φ for sample B and D. SE for sample B is weakly decreasing below 1: pump induced absorption is present. Instead, in sample D, SE > 1 and reaches a maximum of 1.22 (0.43 dB/cm) at a power density of hundreds of W/cm^2. For higher pump power SE decreases due to CA. Note that in Ref. [19] for sample B we were able to achieve a maximum SE = 1.06 (0.12 dB/cm), at one order of magnitude higher photon flux while pumping with a wavelength of 488 nm, i.e. resonantly with an Er^{3+} absorption band.

It is possible to correct the SE data from the CA losses. By doing that, we measured the SE at 1600 nm and divided the SE data measured at 1535 nm by this quantity. As a result we obtain a maximum SE of 1.30 (1.12 dB/cm) for sample D that means an internal gain of 0.56 dB/cm (0.13 cm^{-1}) at $\Phi = 1.4 \times 10^{21}$ photon/s cm^2. This value is significantly higher than 0.2 dB/cm found in sample B pumped with 488 nm light at the same photon flux [19]: it is worth noting that σ_{exc} and σ_{abs} at 488 nm are significantly higher than those at 532 nm, and therefore the increased internal gain in sample D with respect to sample B is even more significant. These values of SE are compatible with excited state ion populations of few percent, which means that a low quantity of erbium is being excited through the nanoclusters [25].

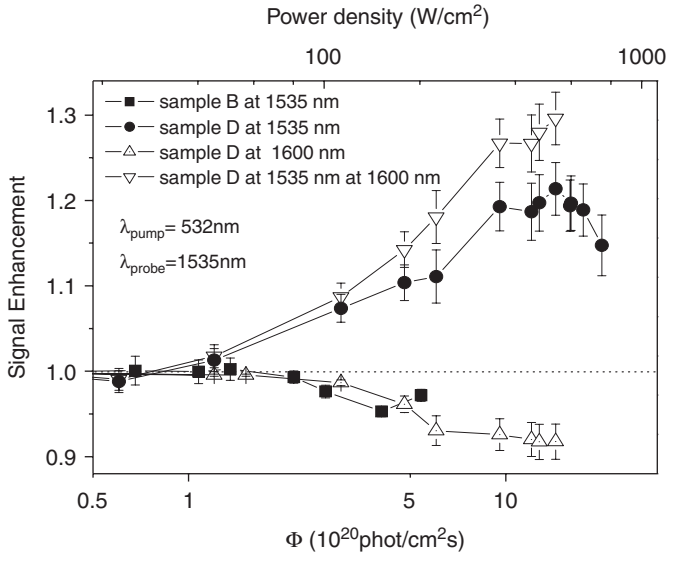

Fig. 6. SE for 1535 nm probe for sample B (black squares) and D (black circles). Empty triangles are the SE measurement at 1600 nm that we take as the CA contribution for sample D and inverted triangles are the result of isolating the contribution of Er^{3+} from the CA absorption. The pump wavelength was 532 nm.

7. Conclusions

We have demonstrated that a reduction of the annealing time, while keeping constant all the other processing parameters, has significantly improved the performances in terms of signal enhancement between Si-nc and Er^{3+} at high pump powers. The phenomena which prevent us to get overall gain in the waveguides are on one side confined carrier absorption (CA) which introduces a loss mechanism and quenches the Si-nc to Er energy transfer and the low erbium fraction coupled to the Si-nc. It seems that the reduced annealing time affects mainly the formation of large Si-nc reducing the effects of confined CA. In any case there is still lot of work to do to improve the material system.

Acknowledgement

Financial support by EC under project SINERGIA (FP5-29650) and LANCER (FP6-033574) is acknowledged.

References

[1] W.J. Miniscalco, J. Lightwave Technol. 9 (1991) 234.
[2] P.C. Becker, N.A. Olsson, J.R. Simpson, Erbium-Doped Fiber Amplifiers, in: Academic Press (Ed.), Fundamentals and Technology. Academic Press, New York, 1999.
[3] J. Kenyon, Semicond. Sci. Technol. 20 (2005) R65.
[4] A.J. Kenyon, P.F. Trwoga, M. Federighi, C.W. Pitt, J. Phys. Condens. Matter 6 (1994) L319.
[5] M. Fujii, M. Yoshida, Y. Kanzawa, S. Hayashi, K. Yamamoto, Appl. Phys. Lett. 71 (1997) 1198.
[6] G. Franzò, V. Vinciguerra, F. Priolo, Appl. Phys. A: Mater. Sci. Process. A 69 (1999) 3.
[7] J.H. Shin, S.-Y. Seo, S. Kim, S.G. Bishop, Appl. Phys. Lett. 76 (2000) 1999.
[8] P.G. Kik, M.L. Brongersma, A. Polman, Appl. Phys. Lett. 76 (2000) 2325.
[9] F. Priolo, G. Franzò, D. Pacifici, V. Vinciguerra, F. Iacona, A. Irrera, J. Appl. Phys. 89 (2001) 264.
[10] K. Watanabe, H. Tamaoka, M. Fujii, K. Moriwaki, S. Hayashi, Physica E 13 (2002) 1038.
[11] M. Fujii, K. Imakita, K. Watanabe, S. Hayashi, J. Appl. Phys. 95 (2004) 272.
[12] F. Iacona, D. Pacifici, A. Irrera, M. Miritello, G. Franzò, F. Priolo, Appl. Phys. Lett. 81 (2002) 3242.

[13] F. Gourbilleau, C. Dufour, M. Levalois, J. Vicens, R. Rizk, C. Sada, F. Enrichi, G. Battaglin, J. Appl. Phys. 94 (2003) 3869.
[14] F. Gourbilleau, M. Levalois, C. Dufour, J. Vicens, A. Rizk, J. Appl. Phys. 95 (2004) 3717.
[15] P.K. Tien, Appl. Opt. 10 (1971) 2395.
[16] Y. Song, T. Sakurai, K. Kishimoto, K. Maruta, S. Matsumoto, K. Kikuchi, Thin Solid Films 334 (1998) 92.
[17] W. Theiβ, Surf. Sci. Rep. 29 (1997) 91.
[18] A.M. Jayannavar, N. Kumar, Phys. Rev. B 44 (1991) 12014.
[19] N. Daldosso, D. Navarro-Urrios, M. Melchiorri, L. Pavesi, F. Gourbilleau, M. Carrada, R. Rizk, C. García, P. Pellegrino, B. Garrido, L. Cognolato, Appl. Phys. Lett. 87 (2005) 261103.
[20] N. Daldosso, D. Navarro-Urrios, M. Melchiorri, L. Pavesi, C. Sada, F. Gourbilleau, M. Carrada, R. Rizk, Appl. Phys. Lett. 88 (2006) 161901.
[21] C. García, Optical amplification in the visible and infrared, in waveguides containing Si nanoclusters, Ph.D. Thesis, Universitat de Barcelona, 2006.
[22] W.J. Miniscalco, R.S. Quimby, Opt. Lett. 16 (1991) 258.
[23] H.S. Han, S.Y. Seo, J.H. Shin, Appl. Phys. Lett. 79 (2001) 4568.
[24] P.G. Kik, A. Polman, in: L. Pavesi, et al. (Eds.), Towards the first silicon laser, NATO Science Series II, vol. 93, Kluwer, Dordrecht, 2003, p. 383.
[25] C. García, Y. Lebour, P. Pellegrino, J. Carreras, B. Garrido, F. Gourbilleau, R. Rizk, J. Luminescence EMRS—Symposium D issue, doi:10.1016/j.lumin.2006.07.026.